

# Properties of low-lying states in some high nuclearity Mn, Fe and V clusters: Exact Studies of Heisenberg Models

C. Raghu<sup>1</sup>, Indranil Rudra<sup>1</sup>, Diptiman Sen<sup>2</sup> and S. Ramasesha<sup>1</sup>

<sup>1</sup> Solid State and Structural Chemistry Unit, Indian Institute of Science, Bangalore 560012, India

<sup>2</sup> Centre for Theoretical Sciences, Indian Institute of Science, Bangalore 560012, India

## ABSTRACT

Using an efficient numerical scheme that exploits spatial symmetries and spin parity, we have obtained the exact low-lying eigenstates of exchange Hamiltonians for the high nuclearity spin clusters, Mn<sub>12</sub>, Fe<sub>8</sub> and V<sub>15</sub>. The largest calculation involves the Mn<sub>12</sub> cluster which spans a Fock space of a hundred million. Our results show that the earlier estimates of the exchange constants need to be revised for the Mn<sub>12</sub> cluster to explain the level ordering of low-lying eigenstates. In the case of the Fe<sub>8</sub> cluster, correct level ordering can be obtained which is consistent with the exchange constants for the already known clusters with butterfly structure. In the V<sub>15</sub> cluster, we obtain an effective Hamiltonian that reproduces exactly, the eight low-lying eigenvalues of the full Hamiltonian.

PACS numbers: 75.50.Xx, 61.46.+w

## I. INTRODUCTION

The synthesis of high nuclearity transition metal complexes has provided a new dimension to the field of nanomagnetism.<sup>1</sup> Many interesting phenomena have been observed in these systems. Amongst the most exciting are the observation of quantum resonance tunneling and quantum interference<sup>2</sup> in some of these clusters. For example, in the case of the Mn<sub>12</sub> cluster, the ground state with total spin  $S_G = 10$  of the exchange Hamiltonian, under the influence of a large single ion anisotropy gives rise to a manifold of doubly degenerate states with nonzero  $M_s$  values, with  $M_s = \pm 10$  being the lowest energy states. The application of a magnetic field splits the degeneracy of the  $M_s = \pm 10$  states. Varying the magnetic field brings states with  $|M_s| \neq 10$  closer in energy to the higher of the two states with  $|M_s| = 10$ . The weak spin dipolar interactions that exist in the system can connect these nearly degenerate states with different  $M_s$  values, leading to tunneling between the states. This is reflected in experiments as jumps in magnetization in the magnetization *vs* magnetic field plots, whenever the resonance condition is satisfied and as plateaus for off-resonance field values. Similar plateaus are also observed in the V<sub>15</sub> cluster<sup>3</sup>, although the reason for the plateaus in this system is qualitatively different. The quantum interference phenomena observed in the Fe<sub>8</sub> cluster is because the paths connecting the  $M_s = +10$  and  $M_s = -10$  could interfere in the presence of a magnetic field, leading to an oscillation in the tunneling probabilities.<sup>4</sup>

These clusters, at a very basic level are characterized by multidentate ligands interconnecting the transition metal ions. In the clusters, a given magnetic ion has exchange interactions of either sign with several of its neighbors. Thus, these magnetic clusters often correspond to spin frustrated systems. Because of the rather complex exchange pathways which exist in these systems, it is

difficult to predict a priori even the sign of the exchange constant, let alone its magnitude.<sup>5</sup> Since the site symmetry at the magnetic ions is also usually low because of the multidentate ligands in the system, the orbital degeneracy would be lifted leading to weaker ferromagnetic exchange interactions. Thus one should expect low-spin ground states in these systems. However, because of the frustrations in the exchange pathways, even weak ferromagnetic interactions could lead to higher spin ground states, albeit with rather low spin excitation gaps. It is indeed interesting that the Mn<sub>12</sub> cluster has ferrimagnetic ordering<sup>2</sup> of the spins in its ground state for this reason. The high-spin ground state observed in Fe<sub>8</sub> is, however, attributable entirely to frustration in the antiferromagnetic interactions.<sup>6</sup>

In the case of the Mn<sub>12</sub> cluster, while the ground state spin as well as the lowest excitation gap is established experimentally, it is not at all clear what the magnitude and sign of the exchange interactions in the cluster are. In an earlier study<sup>7</sup>, in order to simplify the calculations, each strongly coupled Mn<sup>III</sup> – Mn<sup>IV</sup> pair was replaced by a composite spin-1/2 object. The resulting model was studied for three different sets of exchange constants. It was observed that the ordering of the energy levels is very sensitive to the variations in the exchange constants.

In the case of the Fe<sub>8</sub> cluster, while model exact calculations<sup>6</sup> were possible because of the smaller dimensions of the Hilbert spaces, the exchange parameters used were very different from those that have been determined recently.<sup>8</sup> Considering the sensitivity of the ordering of the energy levels to values of the exchange constants, it is desirable to redo the calculations using revised estimates of the exchange constants.

The simplest cluster that can be studied exactly is the V<sub>15</sub> cluster. In this cluster it is found that eight low-lying states are well separated from the rest of the spectrum.<sup>9</sup> Most of the low-temperature properties are determined by these eight low-lying states. To undertake serious study of the magnetization behavior of the cluster under the influence of an applied magnetic field, it is necessary to construct an accurate model Hamiltonian for these states.

In this paper, we have studied the low-lying states of Mn<sub>12</sub>, Fe<sub>8</sub> and V<sub>15</sub> clusters using exact diagonalization of the corresponding exchange Hamiltonians. We show that in the case of Mn<sub>12</sub>, earlier estimates of the exchange constants fail to provide the ground and excited state spin quantum numbers in agreement with experiments. We have also estimated the most likely exchange constants that give good agreement with experiments. In the case of the Fe<sub>8</sub> cluster, we have studied the properties of the cluster for more recent estimates of the exchange constant. In the case of V<sub>15</sub> we have obtained an effective Hamiltonian for the low-lying states that reproduces the energy level ordering of the eight low-lying states exactly. Such a Hamiltonian would be important in the context of hysteresis studies of the system at low temperatures.

In the next section, we outline the numerical method for obtaining the low-lying states of exchange coupled spin systems which span large Hilbert spaces. In Sec. 3, we discuss the results obtained from this technique for the three magnetic clusters mentioned above, and we summarize our results in Sec. 4.

## II. MODEL HAMILTONIAN AND COMPUTATION DETAILS

The model Hamiltonian employed in these studies is the isotropic exchange Hamiltonian involving exchange interactions between nearest neighbors,

$$\hat{H} = \sum_{\langle ij \rangle} J_{ij} \hat{s}_i \cdot \hat{s}_j , \quad (1)$$

where the exchange interaction  $J_{ij}$  takes the values dictated by experimental studies of structure and magnetic properties. The total dimensionality of the Fock space of the cluster is given by

$$D_F = \prod_{i=1}^n (2S_i + 1), \quad (2)$$

where  $n$  is the total number of spins in the cluster and  $S_i$  is the spin on each ion. In the case of the  $Mn_{12}$  cluster consisting of eight spin-2 ions and four spin-3/2 ions, the Fock space dimensionality is a hundred million. Specializing to a given total  $M_S$  leads to Hilbert space dimensionalities which are lower than the Fock space dimensionality. In the case of the  $Mn_{12}$  cluster the  $M_S = 0$  space has a dimensionality of over eight million (8,581,300). The major challenge in exact computation of the eigenvalues, and properties of these spin clusters lies in handling such large basis and the associated matrices. While the dimensions look overwhelming, the matrices that represent the operators in these spaces are rather sparse. Usually, the number of nonzero elements in a row is of the order of the number of exchange constants in the Hamiltonian. This sparseness of the matrices allows one to handle fairly large systems. However, in the case of spin problems, generating the basis states and using the symmetries of the problem is nontrivial.

The isotropic exchange Hamiltonians conserve the total spin,  $S$ , besides the  $z$ -component of the total spin,  $M_S$ . Besides these symmetries, the geometry of the cluster also leads to spatial symmetries which can often be exploited. The simplest way of generating basis functions which conserve total spin is the VB method that employs the Rumer-Pauling rule.<sup>10</sup> It is quite easy to generalize the Rumer-Pauling rules to a cluster consisting of objects with different spins to obtain states with desired total spin,  $S$ . However, setting up the Hamiltonian matrix in such a basis can be computer intensive since the exchange operators operating on a "legal" VB diagram (diagram that obeys Rumer-Pauling rules) can lead to "illegal" VB diagrams, and resolving these "illegal" VB diagrams into "legal" diagrams would present the major bottle-neck. Indeed, the same difficulty is encountered when spatial symmetry operators operate on a VB function. Thus, the extended VB methods are not favored whenever one wishes to apply it to a motley collection of spins or when one wishes to exploit some general spatial symmetries that may exist in the cluster.

Usually, in frustrated spin systems, it is important to partition the spaces into different total spin spaces because of the usually small energy gaps between total spin states which differ in  $S$  by unity. To avoid the difficulties involved in working with total spin eigenfunctions, we exploit parity symmetry in the systems. The parity operation involves changing the  $z$ -component of all the spins in the cluster from  $M_{S_i}$  to  $-M_{S_i}$ . There is an associated phase factor with this operation given by  $(-1)^{S_{tot} + \sum_i S_i}$ . The isotropic exchange operator remains invariant under this operation. If this symmetry is employed in the  $M_S = 0$  subspace, the subspace is divided into "even" and "odd" parity spaces depending upon the sign of the character under the irreducible representation of the parity group. The space which corresponds to even (odd) total spin we call the even (odd) parity space. Thus, employing parity allows partial spin symmetry adaptation which separates successive total spin spaces, without introducing the complications encountered in the VB basis. However, the VB method can lead to complete factorization of the spin space leading to smaller complete subspaces.

In the  $Mn_{12}$  cluster, besides spin symmetries, there also exists spatial symmetries. The topology of the exchange interaction leads to a  $C_4$  point group symmetry. At first sight, this point group appears to present difficulties because the characters in the irreducible representation are in some cases complex. This could lead to complex basis functions. This, however, can be avoided by recognizing that in the  $C_n$  group, states with wave vectors  $k$  and  $-k$  are degenerate in the absence of an external magnetic field. We can therefore construct a linear combination of the  $k$  and  $-k$  states which is real. The symmetry representations in the  $C_4$  group would then correspond to

the labels  $A$ ,  $B$  and  $E$ , with the characters in the  $E$  representation given by  $2\cos(rk)$  under the symmetry operation  $C_4^r$ , with  $k = \pi/2$ . The parity operation commutes with the spatial symmetry operations, and the full point group of the system would then correspond to the direct product of the two groups. Since both parity and spatial symmetries can be easily incorporated in a constant  $M_S$  basis, we do not encounter the difficulties endemic to the VB theory.

The generation of the complete basis in a given Hilbert space requires a simple representation of a state on the computer. This is achieved by associating with every state a unique integer. In this integer, we associate  $n_i$  bits with spin  $s_i$ , such that  $n_i$  is the smallest integer for which  $2^{n_i} \geq 2s_i + 1$ . In the integer that represents the state of the cluster, we ensure that these  $n_i$  bits do not take values which lead to the  $n_i$ -bit integer value exceeding  $2s_i + 1$ . For each of the allowed bit states of the  $n_i$ -bit integer, we associate an  $M_{S_i}$  value between  $-s_i$  and  $s_i$ . For a spin cluster of  $n$  spins, we scan all integers of bit length  $N = \sum_{i=1}^n n_i$  and verify if it represents a basis state with the desired  $M_S$  value. In Fig. 1, we show a few basis functions with specified  $M_s$  value for some typical clusters along with their bit representations and the corresponding integers. Generation of the basis states is usually a very fast step, computationally. Generating the basis as an ordered sequence of integers that represent them also allows for a rapid generation of the Hamiltonian matrix elements as will be seen later.

Symmetrization of the basis by incorporating parity and spatial symmetries involves operating on the constant  $M_S$  basis by the symmetry operators. Since spatial symmetry operators exchange the positions of equivalent spins, every spatial symmetry operator operating on a basis function generates another basis function. Every symmetry operator can be represented by a correspondence vector whose  $i^{\text{th}}$  entry gives the state that results from operating on the  $i^{\text{th}}$  state by the chosen operator. This is also true for the parity operator, in the  $M_S = 0$  subspace. The symmetry combinations can now be obtained by operating on each state by the group theoretic projection operator,

$$\hat{P}_{\Gamma_i} = \frac{1}{h} \sum_R \chi_{\Gamma_i}(R) \hat{R} \quad (3)$$

on each of the basis states. Here  $\Gamma_i$  is the  $i^{\text{th}}$  irreducible representation,  $\hat{R}$  is the symmetry operation of the group,  $h$  is the order of the symmetry group, and  $\chi_{\Gamma_i}(R)$  is the character under  $\hat{R}$  in the irreducible representation  $\Gamma_i$ . The resulting symmetrized basis is overcomplete. The linear dependencies can be eliminated by a Gram-Schmidt orthonormalization procedure. However, in most cases, ensuring that a given basis function does not appear more than once in a symmetrized basis is sufficient to guarantee linear independence and weed out the linearly dependent states. A good check on the procedure is to ensure that the dimensionality of the symmetrized space agrees with that calculated from the traces of the reducible representation obtained from the matrices corresponding to the symmetry operators. Besides, the sum of the dimensionalities of the symmetrized spaces should correspond to the dimensionality of the unsymmetrized Hilbert space.

The generation of the Hamiltonian matrix is rather straightforward and involves operation of the Hamiltonian operator on the symmetry adapted basis. This results in the matrix  $\mathbf{SH}$ , where  $\mathbf{S}$  is the symmetrization matrix representing the operator  $\hat{P}_{\Gamma_i}$  and  $\mathbf{H}$  is the matrix whose elements  $h_{ij}$  are defined by

$$\hat{H}|i\rangle = \sum_j h_{ij}|j\rangle. \quad (4)$$

The states  $i$  correspond to the unsymmetrized basis functions. The Hamiltonian matrix in the symmetrized basis is obtained by right multiplying the matrix  $\mathbf{SH}$  by  $\mathbf{S}^\dagger$ . The symmetric Hamilto-

nian matrix is stored in the sparse matrix form and the matrix eigenvalue problem is solved using the Davidson algorithm.

Computation of the properties is easily done by transforming the eigenstate in the symmetrized basis into that in the unsymmetrized basis. Since the operation by any combination of spin operators on the unsymmetrized basis can be carried out, all relevant static properties in different eigenstates can be obtained quite simply.

### III. RESULTS AND DISCUSSION

We have solved the exchange Hamiltonian exactly for the  $\text{Mn}_{12}$ ,  $\text{Fe}_8$  and  $\text{V}_{15}$  clusters using the above mentioned method. We have obtained the eigenvalues and various properties of the eigenstates such as spin densities and spin-spin correlation functions for these clusters. In what follows, we will discuss these in detail.

#### A. $\text{Mn}_{12}\text{Ac}$ Cluster

In Fig. 2 we show the geometry and the exchange parameters for this cluster. The crystal structure suggests that the exchange constant  $J_1$  is largest and antiferromagnetic in nature.<sup>11</sup> Based on magnetic measurements, it has been suggested that  $J_1$  has a magnitude of 215K. The other magnitude and sign of the other exchange constants are based on comparisons with manganese systems in smaller clusters.<sup>11</sup> It has been suggested that the exchange constant  $J_2$  and  $J_3$  are antiferromagnetic and have a magnitude of about 85K. However, for the exchange constant  $J_4$ , there is no concrete estimate, either of the sign or of the magnitude. In an earlier study, the  $\text{Mn}^{III}$  -  $\text{Mn}^{IV}$  pair with the strongest antiferromagnetic exchange constant was replaced by a composite spin-1/2 object<sup>7</sup>, and the exchange Hamiltonian of the cluster was solved for three different sets of parameters. It was found that the ordering of the energy levels were very sensitive to the relative strengths of the exchange constants. In these studies,  $J_4$  was set to zero and the low-lying excited states were computed. Besides, only states with spin  $S$  up to 10 could be obtained because of the replacement of the higher spin ions by composite spin-1/2 objects.

In our calculation, we have dealt with all the magnetic ions in the cluster and using symmetry, we have factored the  $M_S = 0$  Hilbert space into the six symmetry subspaces. The dimensionalities of the different subspaces is given in Table I. We have obtained low-lying eigenstates in each of these sectors and determined the total spin of the state by explicitly computing the expectation value of the  $\hat{S}^2$  operator in the state.

Our results for the low-lying states are shown in Table II. We note that none of the three sets of parameters studied using an effective Hamiltonian, gives the correct ground and excited states, when an exact calculation is performed. It appears that setting the exchange constant  $J_4$  to zero, cannot yield an  $S = 10$  ground state (Table II, cases A, B and C). When  $J_3$  is equal to or slightly larger than  $J_2$  (cases A and B, Table II), we find a singlet ground state, unlike the result of the effective Hamiltonian in which the ground state has  $S = 8$  and  $S = 0$  respectively. The ground state has spin  $S = 6$ , when  $J_3$  is slightly smaller than  $J_2$  (case C, Table II). In all these cases, the first few low-lying states are found to lie within 20K of the ground state.

When we use the parameters suggested by Chudnovsky<sup>12</sup> (case D, Table II), we obtain an  $S = 10$  ground state separated from an  $S = 9$  first excited state by 223K. This is followed by another  $S = 9$

excited state at 421K. Only when the exchange constant  $J_4$  is sufficiently strongly ferromagnetic (case E, Table II), do we find an  $S = 10$  ground state with an  $S = 9$  excited state separated from it by a gap of 35K, which is close to the value inferred indirectly from experimental results.<sup>13</sup> The second higher excited state has  $S = 8$ , and is separated from the ground state by 62K.

We have explored the parameter space a little further by varying  $J_3$  and  $J_4$ , to see the effect of these exchange constants on the ordering of the energy levels. We find that for  $|J_3| = |J_4|$  and  $J_3$  antiferromagnetic but  $J_4$  ferromagnetic, the ground state is always  $S = 10$  (Table III, cases C, D and E); the first and second excited states are  $S = 9$  and  $S = 8$ , respectively. The lowest excitation gap decreases slowly with increasing magnitude of the exchange constants.

We find that the spin of the ground state is very sensitive to  $J_4$ , for fixed value of  $J_3$ . In the case where  $J_4$  weakly ferromagnetic (Table III, case B), we obtain an  $S = 0$  ground state,  $J_4$  weakly antiferromagnetic we obtain an  $S = 4$  ground state (Table III, case A). This shows that frustrations play a dominant role. If  $J_3$  is also made ferromagnetic, the role of frustration is considerably reduced.

In Figs. 3(a) and 3(b), we show the spin density<sup>14</sup> for the Mn<sub>12</sub> cluster in the ground state for the  $S = 10, M_S = 10$  state. While the manganese ions connected by the strong antiferromagnetic exchange show opposite spin densities, it is worth noting that the total spin density on these two ions is 0.691, well away from the value of 0.5 expected, if these ions were indeed to form a spin-1/2 object. We also note that the spin density at the manganese ion in the middle of the crown is much larger than that at the corners. The spin density in the excited state  $S = 9, M_S = 9$ , also has a similar distribution, although in this state, the symmetry of the spin Hamiltonian is apparently broken [Fig. 3(b)]. The corner ions in the crown no longer have the same spin densities; one pair of opposite corner ions have larger spin densities than the other corner pair. However, since this state is doubly degenerate, there is another state in which the spin densities are related to the spin densities of this state by a 90° rotation. In any experiment involving this state, only an arbitrary linear combination of the two spin densities will be observed. Note also that the large differences in the spin densities for the closely lying excited states is an indication of the large degree of spin frustration in the system.

The small energy gap (35K) between the  $S = 10$  ground state and the  $S = 9$  lowest excited state seems to indicate that, if the  $g$  factors of the Mn ions in the core and crown are different then, an applied magnetic field should mix these spin states. Such a mixing would then be reflected in the quantum resonance tunneling experiments. However, it appears that the experiments are well described by the  $S = 10$  state alone. This is what we should expect from the symmetry of the two low-lying states. We note that the ground state has  $A$  symmetry while the lowest excited state has a  $E$  symmetry. These two states cannot be mixed by any perturbation that retains the  $C_4$  symmetry of the cluster.

## B. Fe<sub>8</sub> Cluster

The Fe<sub>8</sub> cluster is shown in Fig. 4. Each of the Fe ions has a spin of 5/2 and the ground state of the system has a total spin  $S = 10$ , with  $S = 9$  excited state separated from it by about 20K. All the exchange interactions in this system are expected to be antiferromagnetic. While the structure of the complex dictates that the exchange interaction  $J_2$  along the back of the butterfly should be considerably smaller than the interaction  $J_1$  across the wing<sup>15</sup>, in earlier studies it was reported that such a choice of interaction parameters would not provide a  $S = 10$  ground state.<sup>6</sup>

We have carried out exact calculations of the eigenstates of the Fe<sub>8</sub> cluster using four sets of

parameters; the last set of parameters (Case D) are taken from Ref. [17]. In cases A, C and D,  $J_2$  is very much smaller than  $J_1$ . We find that in all the four cases, the ground state has a spin  $S = 10$  and the lowest excited state has spin  $S = 9$ . One of the main differences we find amongst the four sets of parameters is in the energy gap to the lowest excited state (Table IV). For the set of parameters used in the earlier study, this gap is the lowest at 3.4K (case B). For the parameter sets A, C and D<sup>8</sup>, this gap is respectively 13.1K, 39.6K and 42.4K. While in cases A, C and D, the second excited state has spin-9, in case B, this state has spin-8.

The spin densities in all the four cases for both the ground and the excited state are shown in Figs. 5(a) to 5(h). The spin densities in all cases are positive at the corners. In cases A and B, the spin density is negative on the Fe ions on the backbone, and is positive on the remaining two Fe sites.<sup>16,17</sup> However, in cases C and D, the negative and positive spin density sites for the Fe ions in the middle of the edges are interchanged. This is perhaps due to the fact that in cases A and B, the exchange constant  $J_3$  is less than  $J_4$ , while in cases C and D, this is reversed. Thus, a spin density measurement can provide relative strengths of these two exchange constants. In all the cases, the difference between the spin densities in the ground and excited states is that the decrease in the spin density in the excited state is mainly confined to the corner Fe sites. Note that the spin densities in cases C and D are almost the same, although the excitation gaps are significantly different and in proportion to the differences in the exchange constants.

We should note here that the spin densities presented by us are expectation values of the site operators  $S_i^z$  in the  $S = 10, M_S = 10$  and  $S = 9, M_S = 9$  states. However, experimental values are obtained not only at the Fe sites but also at the spin polarized neighboring ligand atom sites. We therefore use the experimental results only as a guideline for locating the negative spin density Fe sites which are sensitive to the set of exchange constants used in the calculation.

The Fe<sub>8</sub> cluster is quite different from the Mn<sub>12</sub> cluster in the following sense. In the Fe<sub>8</sub> cluster, we have excited states of spin  $S = 8$  and  $S = 9$  which have the same symmetry as that of the  $S = 10$  ground state. Furthermore, the total splitting of the ground state due to the anisotropic terms arising in the system due to spin-dipolar interactions is larger than the energy gaps with the  $S = 8$  and  $S = 9$  states of the same spatial symmetry as the ground state. Thus, if the  $g$  factors of the Fe ions on the backbone of the butterfly are different from those on the wings, then an applied magnetic field could lead to mixing between the different spin states. We expect this to provide an additional mechanism for quantum resonance tunneling in the Fe<sub>8</sub> cluster.

### C. V<sub>15</sub> Cluster

The simplest cluster to study is the V<sub>15</sub> cluster, since each of the ions has a spin of half. The interesting aspect of the V<sub>15</sub> cluster is that the three spins sandwiched between the hexagons [Fig. 6] have no direct spin-spin interactions. All the interactions shown in Fig. 6 are antiferromagnetic and the spin system is frustrated. The eigenstates of this system consist of eight states corresponding to the triangle spins (i.e., three spin-1/2 sites) which are split off from the rest of the spectrum. A combination of three two-spin interactions which retains the  $C_3$  symmetry of the molecule is sufficient to account for such a spectrum. We find that the effective Hamiltonian is given by

$$H_{sp-sp} = \epsilon I + \alpha (S_1 \cdot S_2 + S_2 \cdot S_3 + S_3 \cdot S_1), \quad (5)$$

where  $\epsilon = -4.78187$  and  $\alpha = 0.02015$  in units of the exchange  $J_1$ . This Hamiltonian reproduces the eight low-lying eigenstates of the full exchange Hamiltonian to numerical accuracy.

The spin density distribution in one of the  $S = 1/2, M_S = 1/2$  ground states as well as in the  $S = 3/2, M_S = 3/2$  excited state is shown in Figs. 7(a) and 7(b). We find that the spin densities on the hexagons are negligible. The total spin density in the triangle for the  $S = 1/2$  state is nearly equal in value to that of a free electron spin. The  $S = 3/2, M_S = 3/2$  state also has almost equal spin densities at all three sites of the triangle, nearly equal to that of free spins. These observations suggest that describing the low-energy spectrum of this system by the triangle spins is quite appropriate.

#### IV. SUMMARY

To conclude, using a bit representation of the spin states of a spin cluster combined with exploitation of spatial symmetry and spin parity, we are able to obtain model exact solutions for exchange Hamiltonians whose Fock space spans up to a hundred million states. Our studies on the  $\text{Mn}_{12}\text{Ac}$  cluster cluster shows that the earlier effective Hamiltonian studies wrongly estimated the exchange constants. The new exchange constants give the correct spin for the ground state as well as the correct ordering of the low-lying excited states. The spin densities in the cluster also support the fact that the effective Hamiltonian in earlier studies does not accurately represent the cluster. The studies on  $\text{Fe}_8$  cluster shows that the correct ground state as well as the first excited state can be obtained by using a set of exchange constants consistent with the butterfly structure known in related systems, unlike what was concluded in an earlier study. The interesting feature of the  $\text{Fe}_8$  spin densities is that the sites which have negative spin densities depend on the relative strengths of the exchange constants on the sides of the butterfly. In the case of the  $\text{V}_{15}$  cluster, we find that the eight low-lying energy levels can be fitted to an effective Hamiltonian describing three spin-1/2 sites.

### Acknowledgments

We thank the Council of Scientific and Industrial Research, India for financial support through grant No. 01(1595)/99/EMR-II.

---

- <sup>1</sup> T. Lis, *Acta Crystallogr. B* **36**, 2042 (1980); C. Delfas, D. Gatteschi, L. Pardi, R. Sessoli, K. Wieghardt and D. Hanke, *Inorg. Chem.* **32**, 3099 (1993); A. L. Barra, D. Gatteschi, L. Pardi, A. Müller and J. Döring, *J. Am. Chem. Soc.* **114**, 8509 (1992).
- <sup>2</sup> *Quantum Tunneling of Magnetization - QTM'94*, edited by L. Gunther and B. Barbara, NATO ASI Ser. E, Vol. 301 (Kluwer, Dordrecht, 1995); J. R. Friedman, M. P. Sarachik, J. Tejada and R. Ziolo, *Phys. Rev. Lett.* **76**, 3830 (1996); L. Thomas, F. Lioni, R. Ballou, D. Gatteschi, R. Sessoli and B. Barbara, *Nature* **383**, 145 (1996) and references therein; W. Wernsdorfer and R. Sessoli, *Science* **284**, 133 (1999).
- <sup>3</sup> I. Chiorescu, W. Wernsdorfer, A. Müller, H. Böggel and B. Barbara, *Phys. Rev. Lett.* **84**, 15 (2000).
- <sup>4</sup> W. Wernsdorfer and R. Sessoli, *Science* **284**, 133 (1999); A. Garg, *Europhys. Lett.* **22**, 205 (1993) and references therein.
- <sup>5</sup> R. Hotzelmann, K. Wieghardt, U. Flörke, H. Haupt, D. C. Weatherburn, J. Bonvoisin, G. Blondin and J. Girerd, *J. Am. Chem. Soc.* **114**, 1681 (1992).
- <sup>6</sup> C. D. Delfs, D. Gatteschi, L. Pardi, R. Sessoli, K. Wieghardt and D. Hanke, *Inorg. Chem.* **32**, 3099 (1993).
- <sup>7</sup> R. Sessoli, H.-L. Tsai, A. R. Schake, S. Wang, J. B. Vincent, K. Folting, D. Gatteschi, G. Christou and D. N. Hendrickson, *J. Am. Chem. Soc.* **115**, 1804 (1993).
- <sup>8</sup> I. Tupitsyn and B. Barbara, cond-mat/0002180.
- <sup>9</sup> D. Gatteschi, L. Pardi, A. L. Pardi, A. Müller and J. Döring, *Nature* **354**, 465 (1991).
- <sup>10</sup> For a review see, Z. G. Soos and S. Ramasesha, in *Valence Bond Theory and Chemical Structure*, eds. D. J. Klein and N. Trinajstic, Elsevier (1990) p. 81.
- <sup>11</sup> D. N. Hendrickson, G. Christou, E. A. Schmitt, B. Libby, J. S. Baskin, S. Wang, H. L. Tsai, J. B. Vincent, W. P. D. Boyd, J. C. Haffman, K. Folting, Q. Li, W. E. Streib, *J. Am. Chem. Soc.* **114**, 2455 (1992), and references therein.
- <sup>12</sup> E. M. Chudnovsky, *Science* **274**, 938 (1996).
- <sup>13</sup> M. Hennion, L. Pardi, I. Mirebeau, E. Surad, R. Sessoli and A. Caneschi, *Phys. Rev. B*, **56**, 8819 (1997); A. A. Mukhin, V. D. Travkin, A. K. Zvezdin, S. P. Lebedev, A. Caneschi and D. Gatteschi, *Europhys. Lett.* **44**, 778 (1998).
- <sup>14</sup> P. A. Reynolds, E. P. Gilbert and B. N. Figgis, *Inorg. Chem.* **35**, 545 (1996).
- <sup>15</sup> S. M. Gorun and S. J. Lippard, *Inorg. Chem.*, **27**, 149 (1988); W. H. Armstrong, M. E. Roth and S. J. Lippard, *J. Am. Chem. Soc.*, **109**, 6318 (1987).
- <sup>16</sup> Y. Pontillon, A. Caneschi, D. Gatteschi, R. Sessoli, E. Ressouche, J. Schwiezer and E. Lelievre-Berna, *J. Am. Chem. Soc.*, **121**, 5342 (1999).
- <sup>17</sup> A. L. Barra, D. Gatteschi and R. Sessoli, *Chem. Eur. J.*, **6**, 1608 (2000).

Table I: Dimensions of different symmetry subspaces in  $M_s=0$  sector for  $Mn_{12}Ac$ .

Symmetry	Dimension
$^eA$	1074087
$^oA$	1071537
$^eB$	1074037
$^oB$	1071587
$^eE$	2142526
$^oE$	2147526

Table II: Low-Lying states of  $Mn_{12}Ac$ , relative to the ground state for the parameters in question. Entries in parenthesis in cases A, B and C correspond to the effective Hamiltonian results of Sessoli *et al.*<sup>7</sup> Case D corresponds to the parameters suggested by Chudnovsky.<sup>12</sup> The parameters corresponding to different cases are: case (A)  $J_1=225K$ ,  $J_2=90K$ ,  $J_3=90K$ ,  $J_4=0K$ ; case (B)  $J_1=225K$ ,  $J_2=90K$ ,  $J_3=93.8K$ ,  $J_4=0K$ ; case (C)  $J_1=225K$ ,  $J_2=90K$ ,  $J_3=86.2K$ ,  $J_4=0K$ ; case (D)  $J_1=215K$ ,  $J_2=85K$ ,  $J_3=-85K$ ,  $J_4=-45K$ ; case (E)  $J_1=215K$ ,  $J_2=85K$ ,  $J_3=85K$ ,  $J_4=-64.5K$ . All the energies are in K.

Case A	Case B	Case C	Case D	Case E
State S E(K)	State S E(K)	State S E(K)	State S E(K)	State S E(K)
$^eB$ 0 0.0 (8)	$^eB$ 0 0.0 (0)	$^eB$ 6 0.0 (10)	$^eA$ 10 0.0	$^eA$ 10 0.0
$^oE$ 1 10.8 (9) (6.4) (10) (6.4)	$^oE$ 1 16.2 (8) (1.4)	$^oE$ 1 15.5 (8) (2.7)	$^oE$ 9 223	$^oE$ 9 35.1
$^oB$ 1 19.8 (0) (6.8)	$^oB$ 1 20.0	$^oB$ 1 19.6 (9) (5.0)	$^oB$ 9 421.2	$^eB$ 8 62.1
$^eA$ 2 24.7	$^eA$ 2 30.5	$^eA$ 2 23.8	$^oB$ 9 425.1	$^oE$ 7 82.4
$^oE$ 3 39.0	$^eB$ 4 58.4	$^oE$ 1 28.8	$^eB$ 8 439.5	$^eA$ 6 99.7
$^eE$ 2 49.9	$^eE$ 2 60.9	$^eB$ 6 53.6	$^eB$ 8 443.7	$^eB$ 0 102.0
$^eB$ 4 57.1	$^oA$ 3 64.3	$^eB$ 6 54.4	$^eB$ 8 458.1	$^eA$ 2 121.0
$^eB$ 8 57.8	$^eE$ 2 80.0	$^eB$ 8 57.2	$^oA$ 11 573.4	$^oB$ 1 133.3
$^eB$ 2 57.8	$^oA$ 3 88.1	$^eE$ 2 63.0	$^oE$ 9 583.8	$^eE$ 2 177.1
$^oB$ 3 78.4	$^eA$ 6 88.3	$^oA$ 3 77.0	$^eE$ 8 632.8	$^oA$ 3 211.3
$^oB$ 3 86.8	$^oB$ 3 112.8	$^oB$ 3 85.3	$^oA$ 9 640.5	$^oA$ 3 220.8
$^eA$ 6 105.7	$^oB$ 5 114.6	$^eE$ 2 86.1	$^eE$ 8 658.3	$^eE$ 4 249.9
$^oB$ 3 113.4	$^oB$ 5 158.4	$^eA$ 6 97.1	$^eA$ 8 767.1	$^oB$ 5 278.5
$^eE$ 4 117.3	$^oA$ 1 165.2	$^eA$ 6 98.2	$^eB$ 8 807.6	$^oA$ 7 332.1
$^oB$ 5 154.2	$^oA$ 1 181.6	$^oB$ 3 112.2	$^eA$ 8 815.8	$^oA$ 7 340.8

Table III: Low Lying states of  $Mn_{12}Ac$ . The parameters corresponding to different cases are: case (A)  $J_1=215K$ ,  $J_2=85K$ ,  $J_3=85K$ ,  $J_4=45K$ ; case (B)  $J_1=215K$ ,  $J_2=85K$ ,  $J_3=85K$ ,  $J_4=-45K$ ; case (C)  $J_1=215K$ ,  $J_2=85K$ ,  $J_3=64.5 K$ ,  $J_4=-64.5K$ ; case (D)  $J_1=215K$ ,  $J_2=85K$ ,  $J_3=85K$ ,  $J_4=-85K$ ; case (E)  $J_1=215K$ ,  $J_2=85K$ ,  $J_3=45K$ ,  $J_4=-45K$ . All the energies are in K.

Case A	Case B	Case C	Case D	Case E
State S E(K)	State S E(K)	State S E(K)	State S E(K)	State S E(K)
$^eB\ 4\ 0.0$	$^eB\ 0\ 0.0$	$^eA\ 10\ 0.0$	$^eA\ 10\ 0.0$	$^eA\ 10\ 0.0$
$^eA\ 4\ 9.1$	$^oE\ 1\ 12.3$	$^oE\ 9\ 73.7$	$^oE\ 9\ 67.7$	$^oE\ 9\ 80.1$
$^oE\ 3\ 9.4$	$^eA\ 2\ 22.9$	$^eB\ 8\ 135.1$	$^eB\ 8\ 121.2$	$^eB\ 8\ 149.8$
$^eB\ 4\ 18.2$	$^oB\ 1\ 27.6$	$^oE\ 7\ 186.1$	$^oE\ 7\ 165.2$	$^eA\ 8\ 191.0$
$^eA\ 2\ 32.4$	$^oE\ 3\ 28.9$	$^eA\ 8\ 196.0$	$^eA\ 6\ 201.2$	$^oE\ 7\ 210.0$
$^oB\ 5\ 49.4$	$^eB\ 4\ 34.1$	$^eA\ 6\ 227.8$	$^eA\ 8\ 206.5$	$^eA\ 6\ 260.0$
$^eA\ 6\ 50.0$	$^eA\ 10\ 36.5$	$^eB\ 4\ 283.5$	$^eB\ 4\ 247.7$	$^eB\ 4\ 329.8$
$^eE\ 4\ 55.4$	$^eB\ 8\ 37.8$	$^oB\ 1\ 323.0$	$^oB\ 1\ 282.5$	$^oB\ 9\ 346.8$
$^oA\ 3\ 68.2$	$^eE\ 2\ 67.2$	$^eE\ 2\ 364.0$	$^eE\ 2\ 330.2$	$^oB\ 9\ 370.7$
$^oA\ 3\ 70.2$	$^oA\ 3\ 100.1$	$^oA\ 3\ 391.8$	$^oA\ 3\ 365.2$	$^oB\ 1\ 515.8$
$^oB\ 3\ 71.4$	$^oA\ 3\ 119.5$	$^oA\ 3\ 401.6$	$^oA\ 3\ 375.0$	$^eE\ 8\ 400.3$
$^oA\ 3\ 76.6$	$^eA\ 4\ 140.0$	$^eE\ 4\ 420.6$	$^eE\ 4\ 401.9$	$^eE\ 2\ 413.8$
$^eB\ 2\ 255.2$	$^oB\ 3\ 161.8$	$^oB\ 9\ 426.3$	$^oB\ 11\ 421.0$	$^oA\ 5\ 424.2$
$^eB\ 2\ 257.2$	$^oB\ 5\ 172.8$	$^oB\ 5\ 434.9$	$^oB\ 5\ 425.5$	$^oA\ 3\ 432.5$

Table IV: Energies (in units of K) of a few low-lying states in  $Fe_8$ . The exchange constants corresponding to the various cases are: case (A)  $J_1 = 150K$ ,  $J_2 = 25K$ ,  $J_3 = 30K$ ,  $J_4 = 50K$ ; case (B)  $J_1 = 180K$ ,  $J_2 = 153K$ ,  $J_3 = 22.5K$ ,  $J_4 = 52.5K$ ; case (C)  $J_1 = 195K$ ,  $J_2 = 30K$ ,  $J_3 = 52.5K$ ,  $J_4 = 22.5K$ ; case (D)  $J_1 = 201K$ ,  $J_2 = 36.2K$ ,  $J_3 = 58.3K$ ,  $J_4 = 26.1K$ .

Case A	Case B	Case C	Case D
State S E(K)	State S E(K)	State S E(K)	State S E(K)
$^eA\ 10\ 0.0$	$^eA\ 10\ 0.0$	$^eA\ 10\ 0.0$	$^eA\ 10\ 0.0$
$^oB\ 9\ 13.1$	$^oB\ 9\ 3.4$	$^oA\ 9\ 39.6$	$^oA\ 9\ 42.4$
$^oA\ 9\ 26.1$	$^eA\ 8\ 10.2$	$^oB\ 9\ 54.2$	$^oB\ 9\ 58.8$
$^eA\ 8\ 27.3$	$^oB\ 7\ 20.1$	$^oB\ 9\ 62.4$	$^oB\ 9\ 69.4$

## Figure Captions

1. Representative  $M_s = 0$  state in (a) 6 spin-1/2 cluster, (b)  $Mn_{12}Ac$  cluster with first four sites each having spin  $S = 3/2$  and the remaining eight sites each having spin  $S = 2$ . Numbers in parenthesis correspond to the  $M_s = 0$  value at the site. The bit representations as well as the integer values are given just below the diagrams.
2. A schematic diagram of the exchange interactions between the Mn ions in the  $Mn_{12}Ac$  molecule.
3. Spin density of  $Mn_{12}Ac$  for parameter values:  $J_1 = 215K$ ,  $J_2 = 85K$ ,  $J_3 = 85K$  and  $J_4 = -64.5K$ . (a) Spin density for ground state ( $S=10, M_s=10$ ). (b) Spin density for 1<sup>st</sup> excited state ( $S=9, M_s=9$ ).
4. A schematic diagram of the exchange interactions between the Fe ions in the  $Fe_8$  molecule.
5. Spin density of  $Fe_8$  for parameter values:  $J_1 = 150K$ ,  $J_2 = 25K$ ,  $J_3 = 30K$ ,  $J_4 = 50K$ . (a) Spin density for ground state ( $S=10, M_s=10$ ). (b) Spin density for 1<sup>st</sup> excited state ( $S=9, M_s=9$ ). Spin density of  $Fe_8$  for  $J_1 = 180K$ ,  $J_2 = 153K$ ,  $J_3 = 22.5K$ ,  $J_4 = 52.5K$  parameter values. (c) Spin density for ground state ( $S=10, M_s=-10$ ). (d) Spin density for 1<sup>st</sup> excited state ( $S=9, M_s=9$ ). Spin density of  $Fe_8$  for  $J_1 = 195K$ ,  $J_2 = 30K$ ,  $J_3 = 52.5K$ ,  $J_4 = 22.5K$  parameter values. (e) Spin density for ground state ( $S=10, M_s=10$ ). (f) Spin density for 1<sup>st</sup> excited state ( $S=9, M_s=9$ ). Spin density of  $Fe_8$  for  $J_1 = 201K$ ,  $J_2 = 36.2K$ ,  $J_3 = 58.3K$ ,  $J_4 = 26.1K$  parameter values. (g) Spin density for ground state ( $S=10, M_s=10$ ). (h) Spin density for 1<sup>st</sup> excited state ( $S=9, M_s=9$ ).
6. A schematic diagram of the exchange interactions between the V ions in the  $V_{15}$  molecule.
7. Spin density of  $V_{15}$  for  $J_1 = 800K$ ,  $J_2 = 300K$ ,  $J_3 = 150K$  parameter values. (a) Spin density in one of the ground states ( $S=0.5, M_s=0.5$ ). (b) Spin density for excited state ( $S=1.5, M_s=1.5$ ).

(a)

$$\left(\frac{1}{2}\right) \quad \left(-\frac{1}{2}\right) \quad \left(\frac{1}{2}\right) \quad \left(-\frac{1}{2}\right) \quad \left(\frac{1}{2}\right) \quad \left(\frac{1}{2}\right)$$

$$1 \quad 0 \quad 1 \quad 0 \quad 1 \quad 1$$

$$I = 43$$

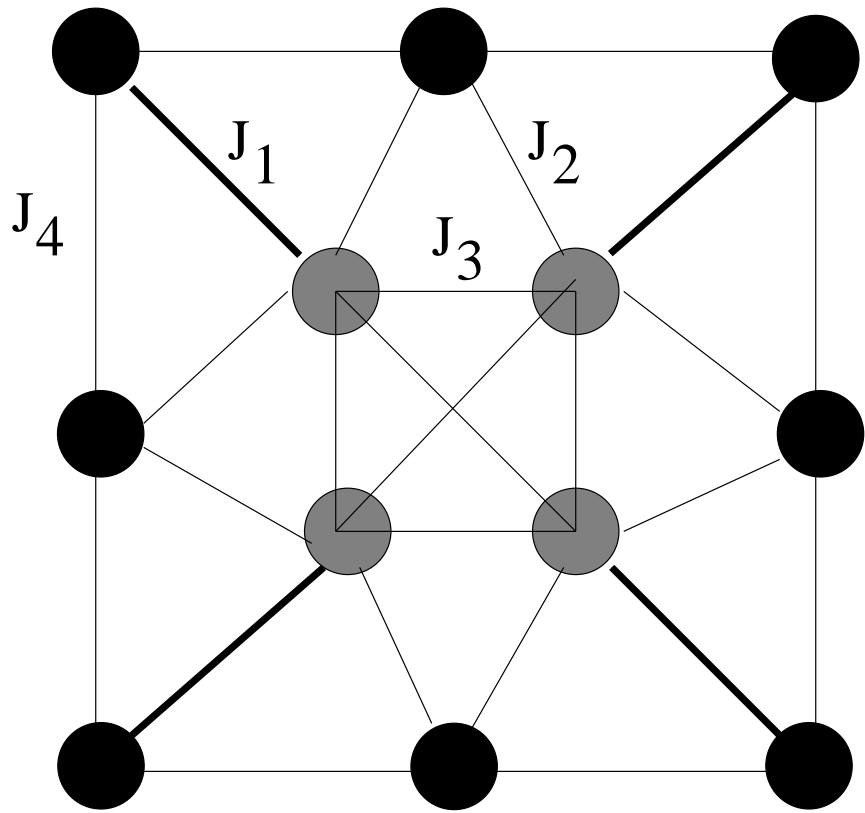
(b)

$$\left(\frac{3}{2}\right) \quad \left(-\frac{3}{2}\right) \quad \left(\frac{3}{2}\right) \quad \left(-\frac{3}{2}\right) \quad (2) \quad (1) \quad (0) \quad (-1) \quad (-2) \quad (0) \quad (-1) \quad (1)$$

$$11 \quad 00 \quad 11 \quad 00 \quad 100 \quad 011 \quad 010 \quad 001 \quad 000 \quad 010 \quad 001 \quad 011$$

$$I = 3431796875$$

Fig. 1



$S = 2$        $S = 3/2$

Fig. 2

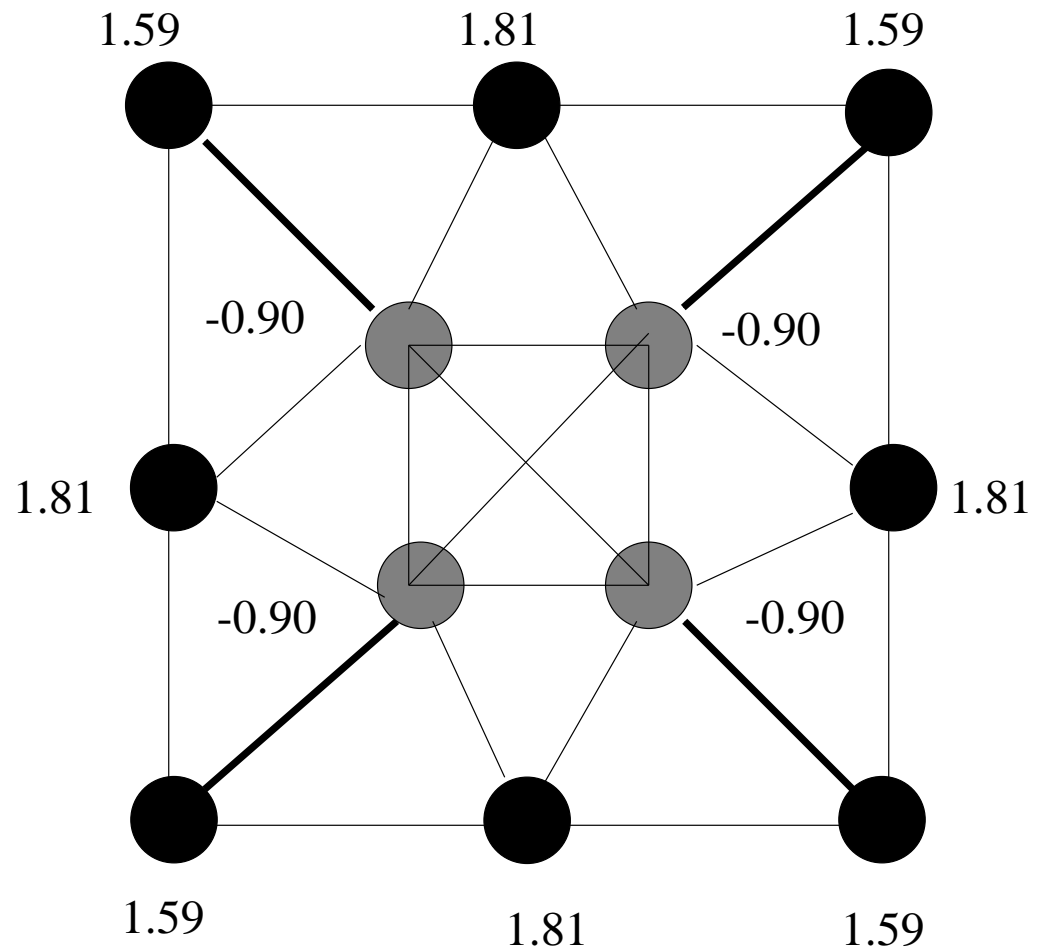


Fig. 3(a)

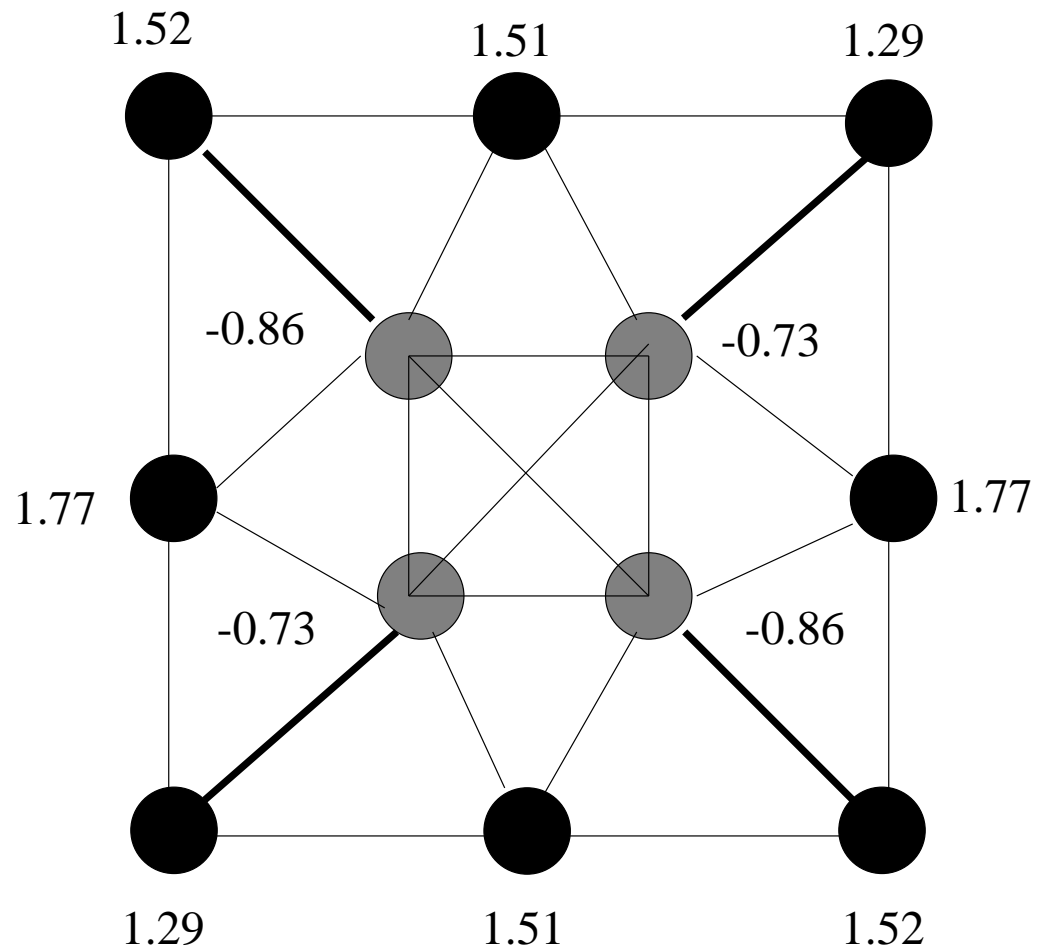


Fig. 3(b)

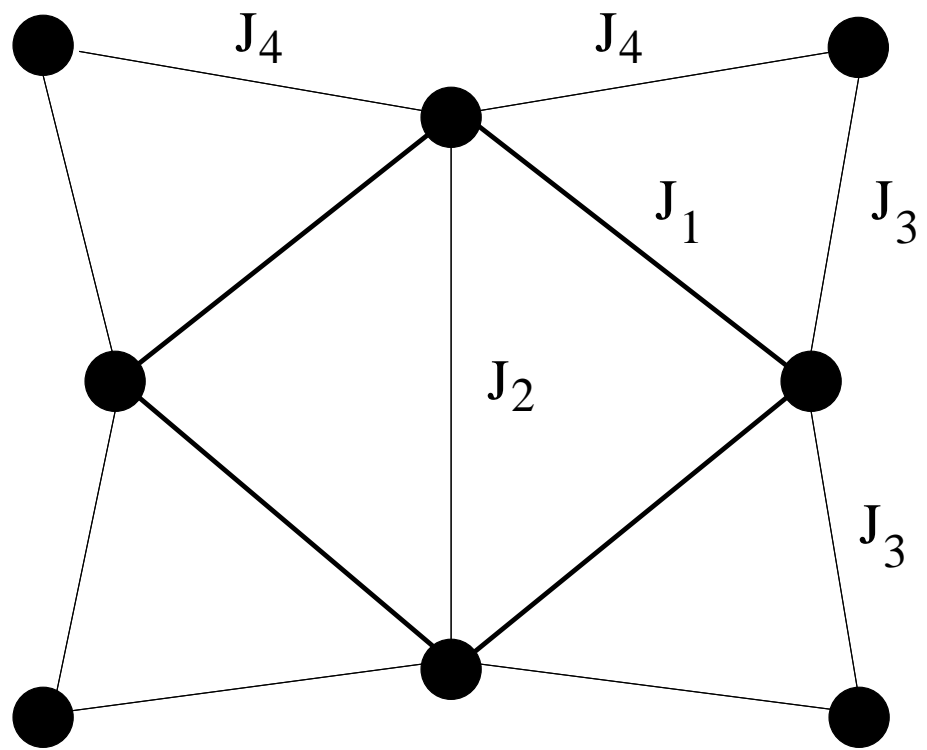


Fig. 4

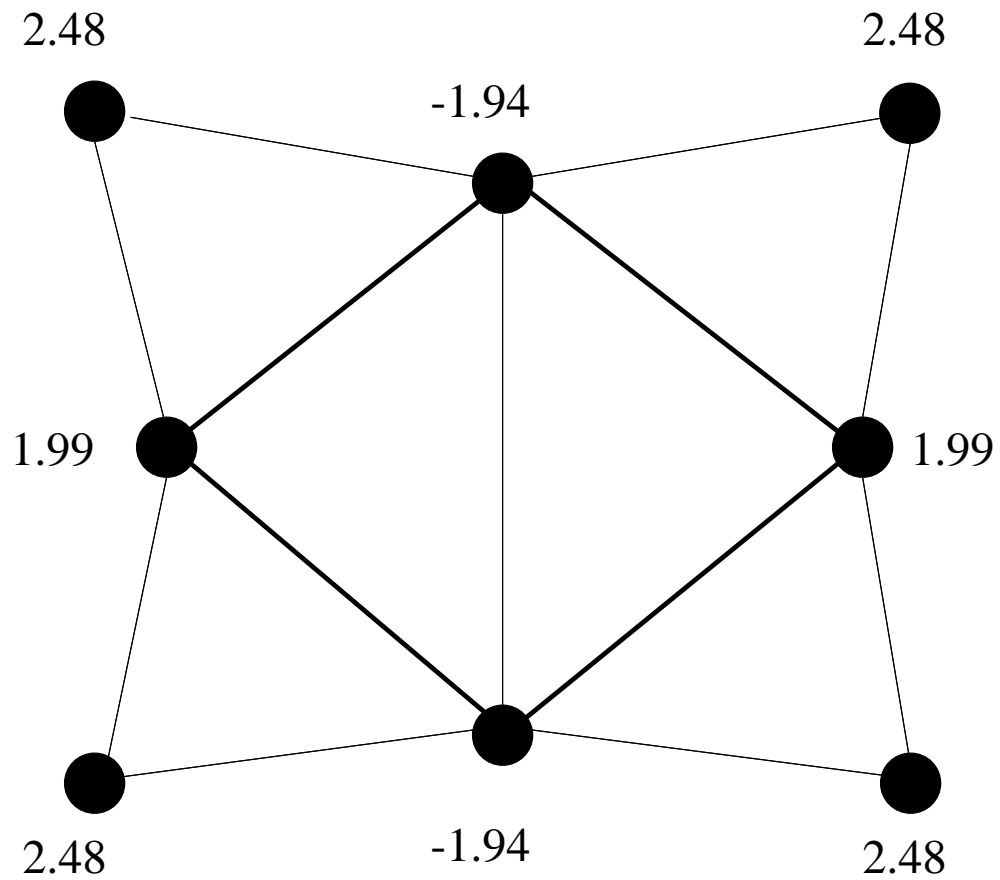


Fig. 5(a)

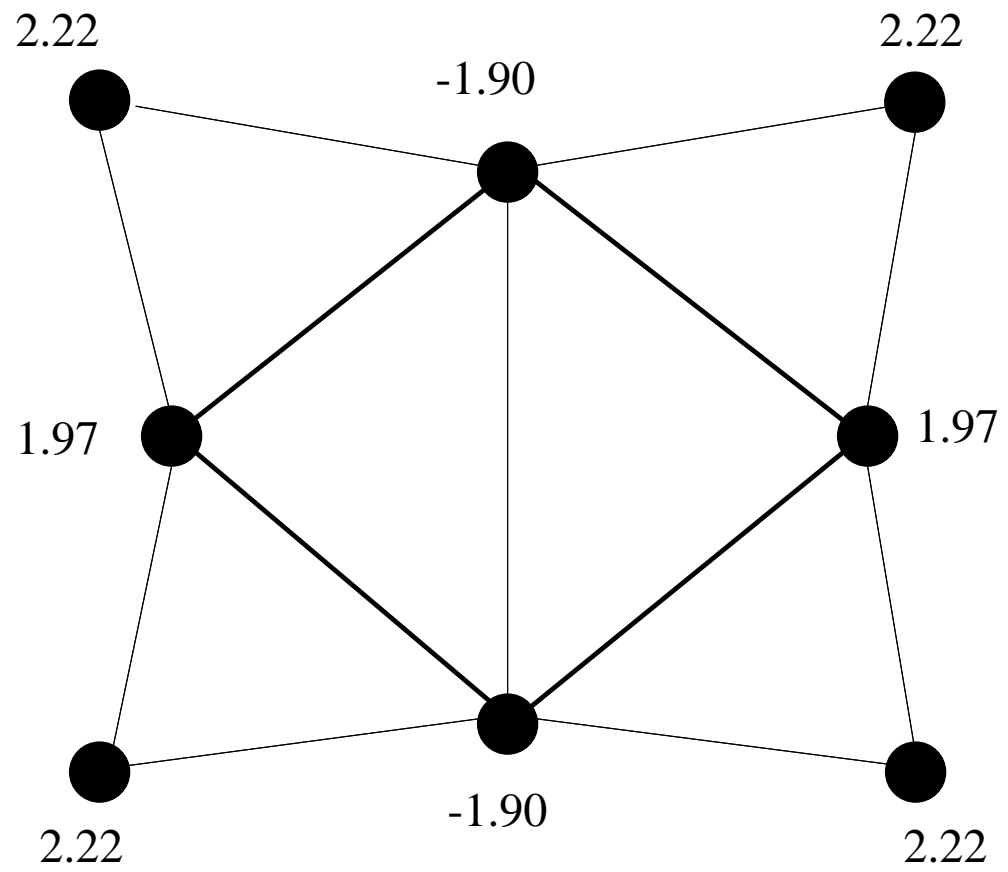


Fig. 5(b)

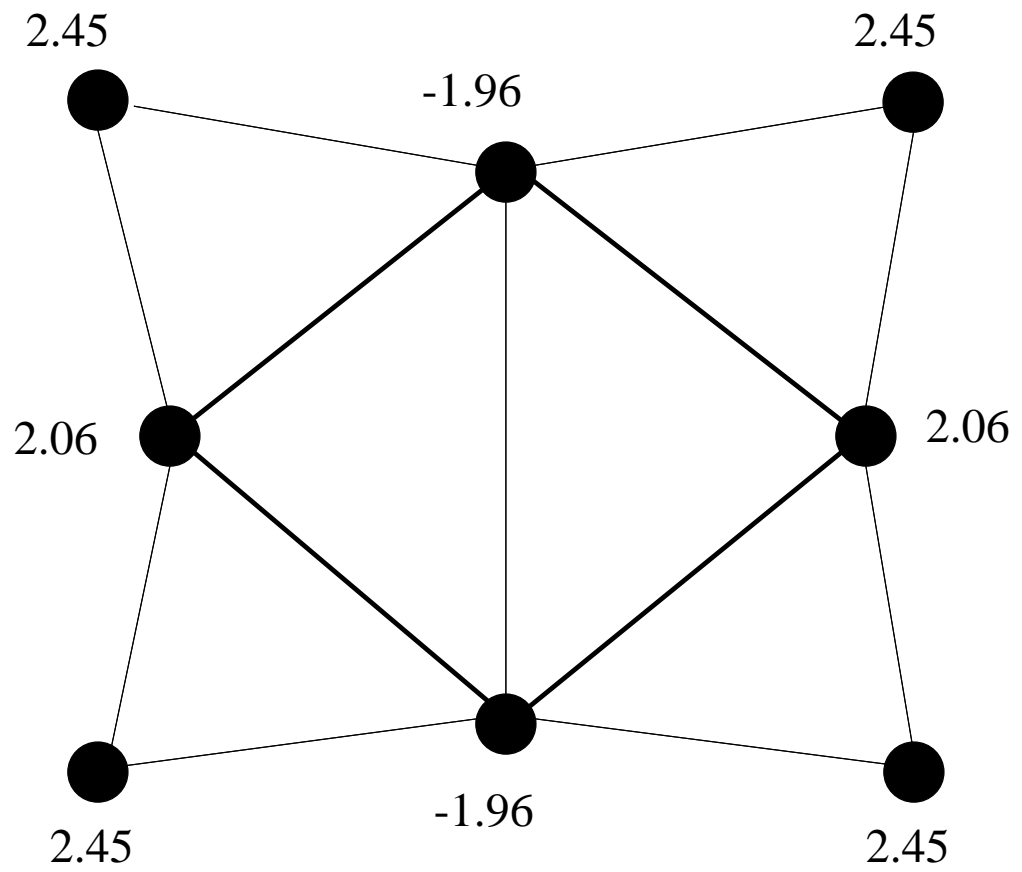


Fig. 5(c)

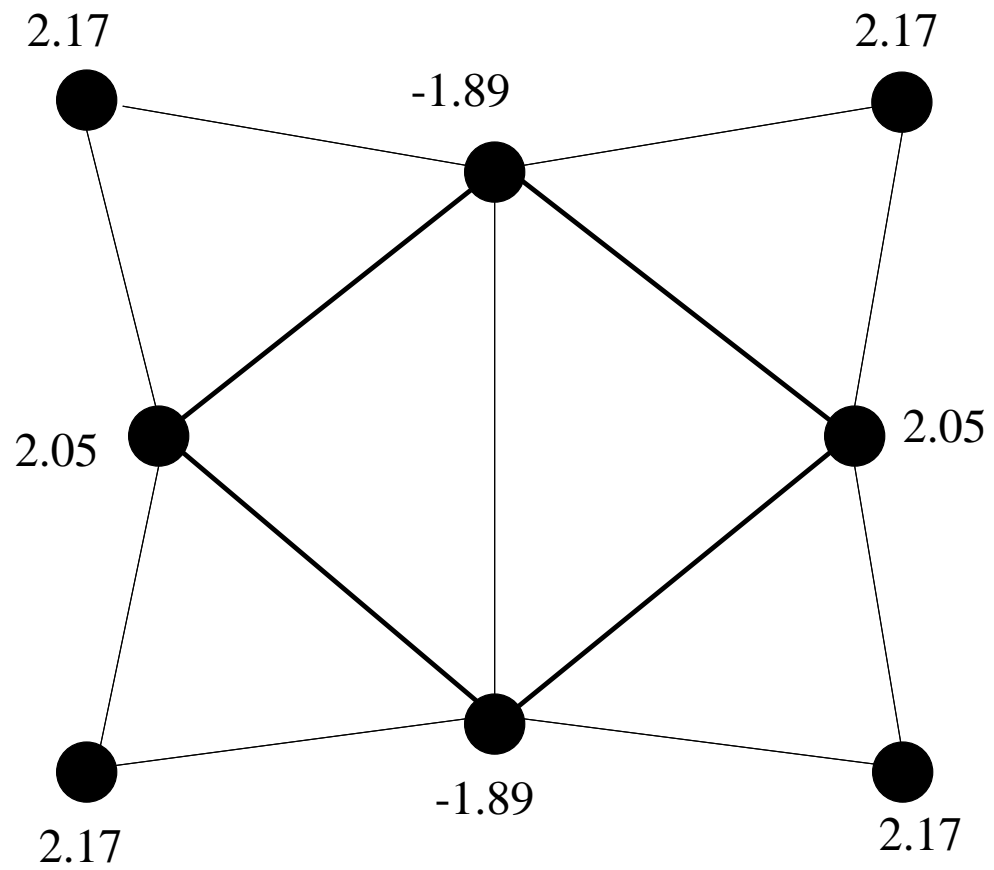


Fig. 5(d)

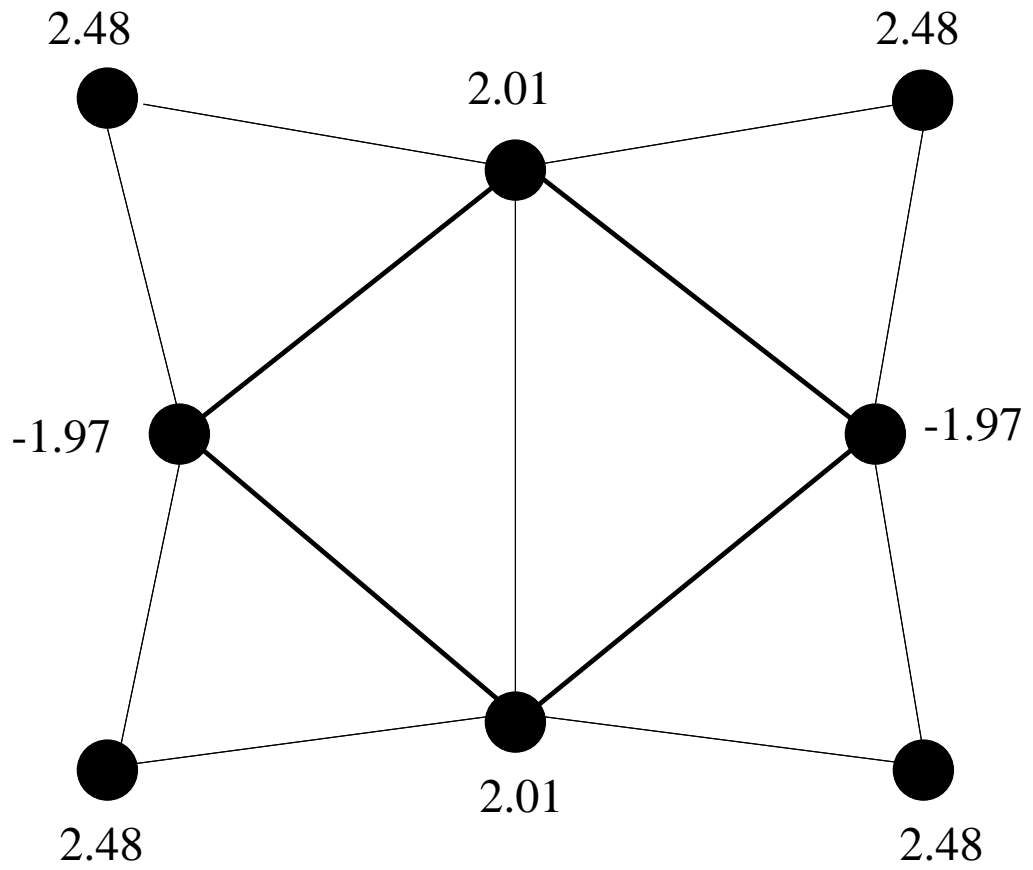


Fig. 5(e)

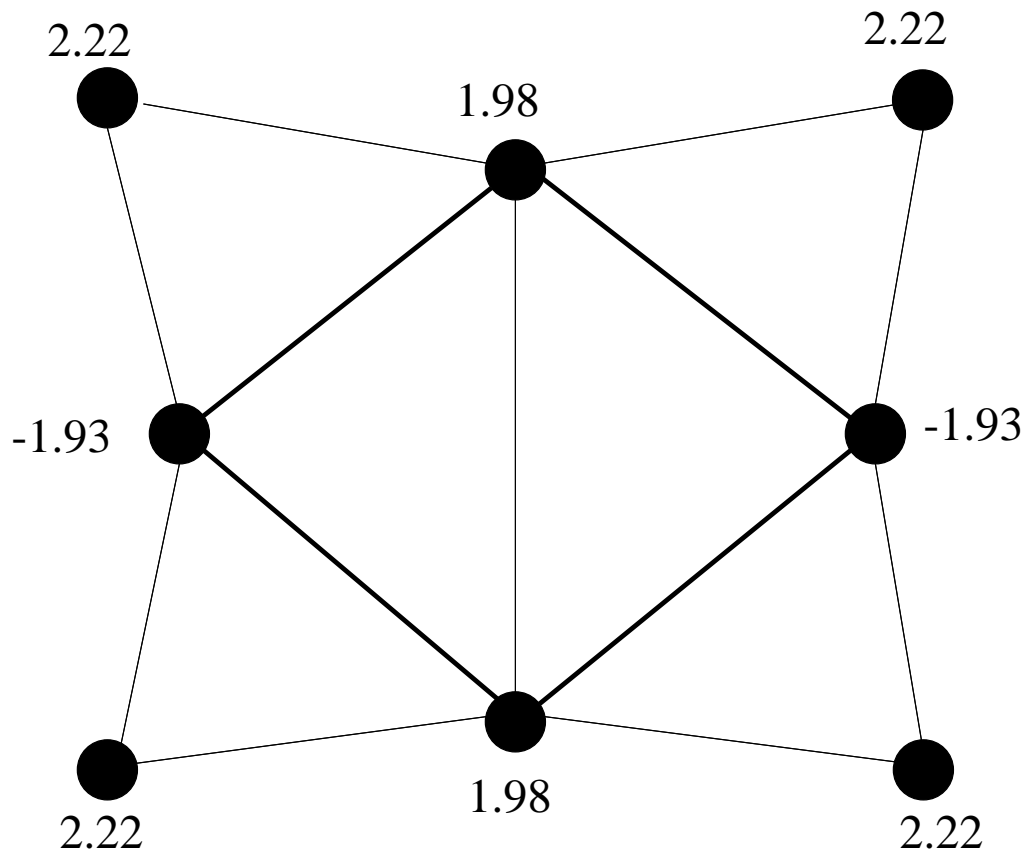


Fig. 5(f)

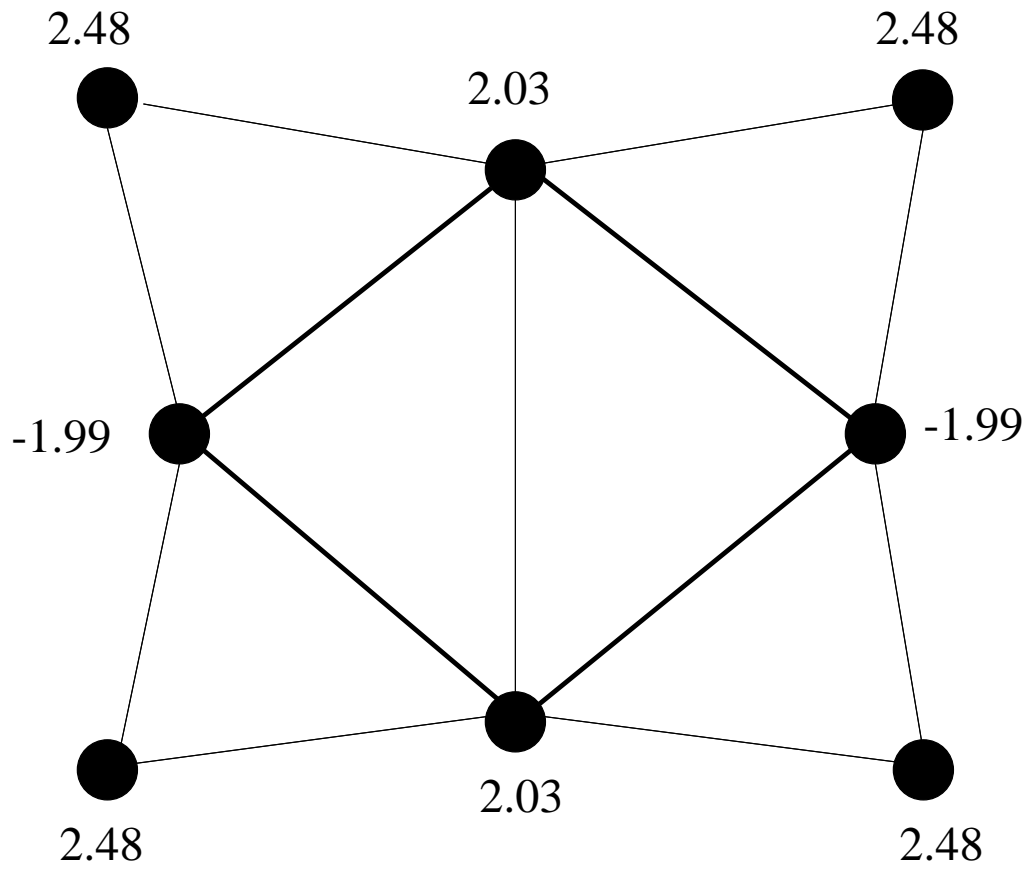


Fig. 5(g)

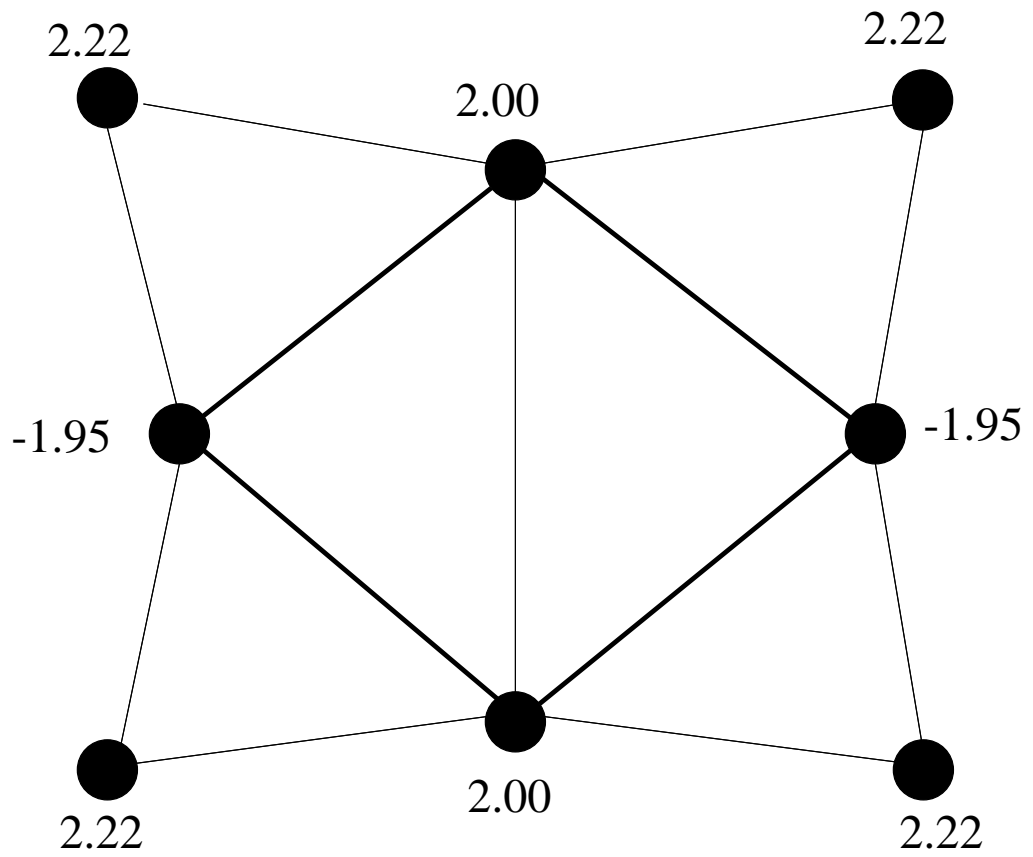
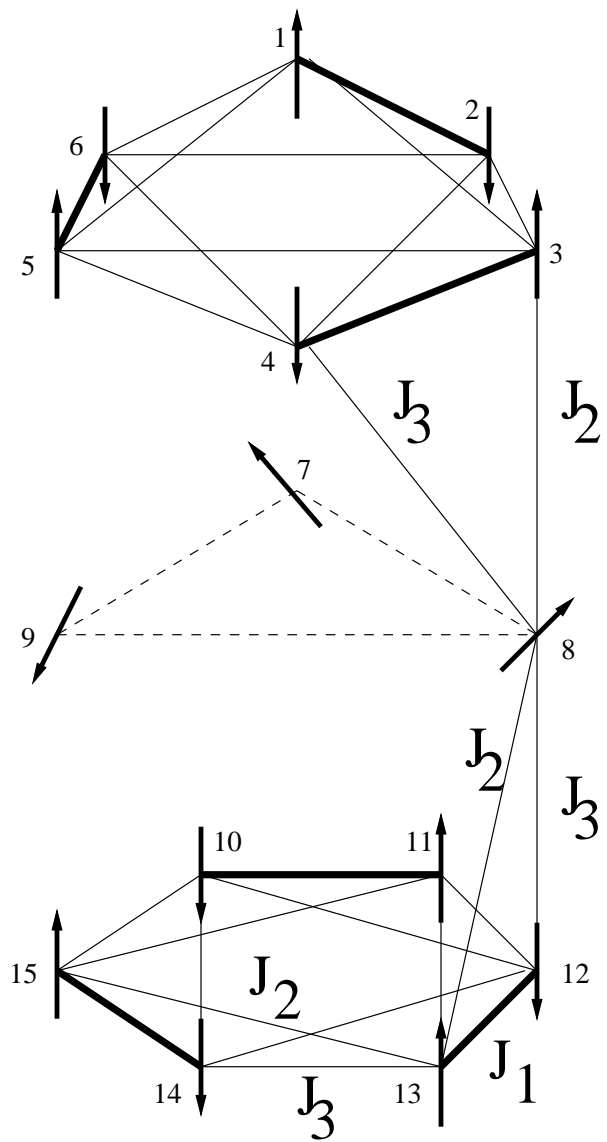


Fig. 5(h)



$$J_1 \sim 800 \text{ K} ; J_2 \sim 300 \text{ K} ; J_3 \sim 150 \text{ K}$$

Fig. 6

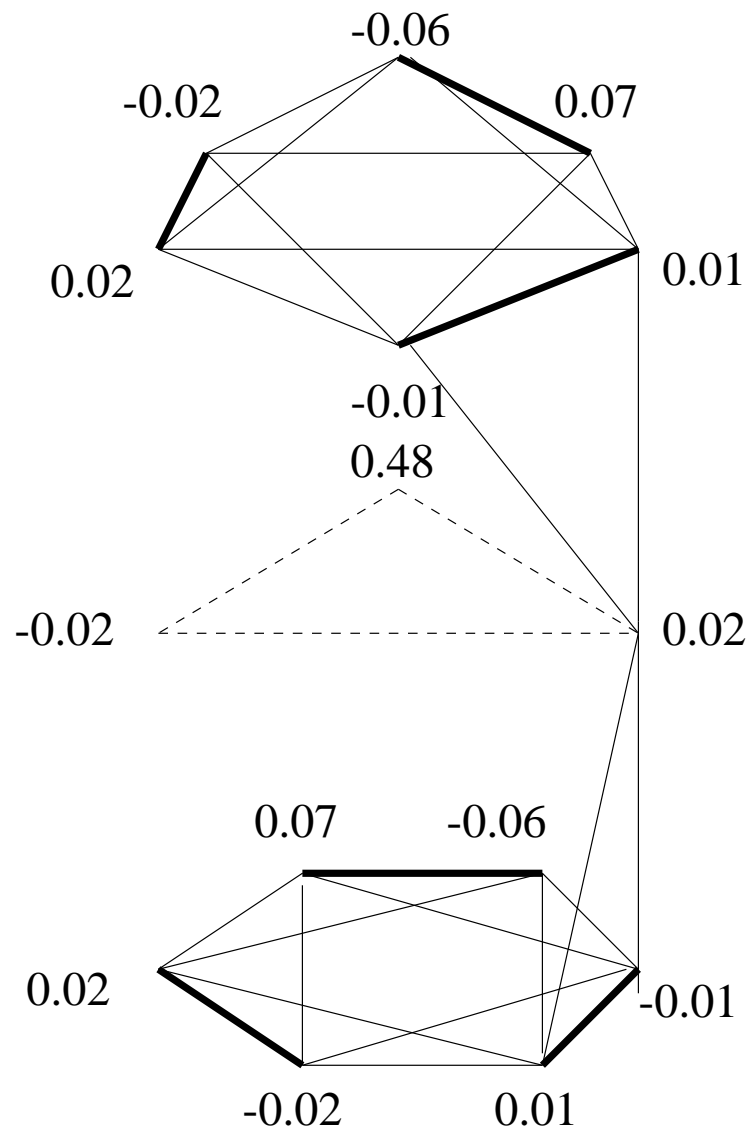


Fig. 7(a)

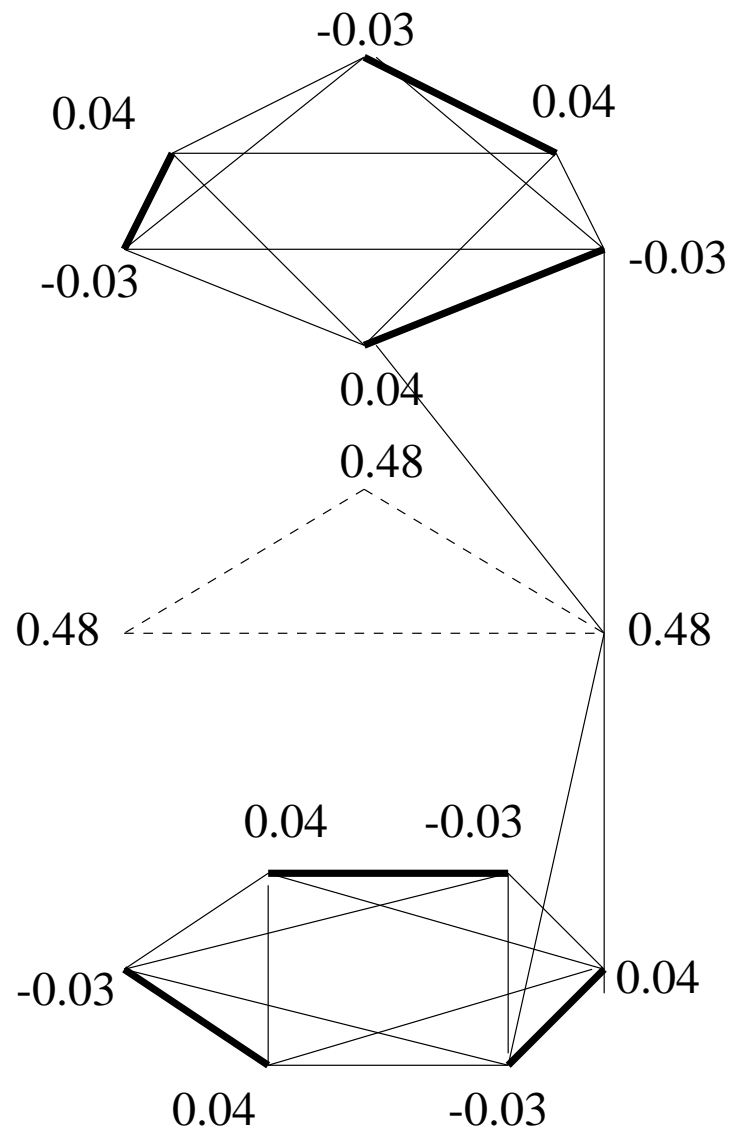


Fig. 7(b)